



HAL
open science

Magnonic Metamaterials for Spin-Wave Control with Inhomogeneous Dzyaloshinskii–Moriya Interactions

Fengjun Zhuo, Hang Li, Zhenxiang Cheng, Aurélien Manchon

► **To cite this version:**

Fengjun Zhuo, Hang Li, Zhenxiang Cheng, Aurélien Manchon. Magnonic Metamaterials for Spin-Wave Control with Inhomogeneous Dzyaloshinskii–Moriya Interactions. *Nanomaterials*, 2022, 12 (7), pp.1159. 10.3390/nano12071159 . hal-03830922

HAL Id: hal-03830922

<https://hal.science/hal-03830922>

Submitted on 26 Oct 2022

HAL is a multi-disciplinary open access archive for the deposit and dissemination of scientific research documents, whether they are published or not. The documents may come from teaching and research institutions in France or abroad, or from public or private research centers.

L'archive ouverte pluridisciplinaire **HAL**, est destinée au dépôt et à la diffusion de documents scientifiques de niveau recherche, publiés ou non, émanant des établissements d'enseignement et de recherche français ou étrangers, des laboratoires publics ou privés.



Distributed under a Creative Commons Attribution 4.0 International License

Magnonic Metamaterials for Spin-Wave Control with Inhomogeneous Dzyaloshinskii–Moriya Interactions

Fengjun Zhuo ^{2,1} , Hang Li ^{1*} , Zhenxiang Cheng ^{3*} , and Aurélien Manchon ^{4*} 

¹ School of Physics and Electronics, Henan University, Kaifeng 475004, China; hang.li@vip.henu.edu.cn

² King Abdullah University of Science and Technology (KAUST), Physical Science and Engineering Division (PSE), Thuwal 23955-6900, Saudi Arabia; fengjun.zhuo@kaust.edu.sa

³ Institute for Superconducting and Electronic Materials, Australian Institute of Innovative Materials, University of Wollongong, Innovation Campus, Squires Way, North Wollongong, NSW 2500, Australia; cheng@uow.edu.au

⁴ Aix Marseille University, CNRS, CINAM, 13288 Marseille, France; aurelien.manchon@univ-amu.fr

* Correspondence: hang.li@vip.henu.edu.cn; cheng@uow.edu.au; aurelien.manchon@univ-amu.fr

Abstract: A magnonic metamaterial in the presence of spatially modulated Dzyaloshinskii–Moriya interaction is theoretically proposed and demonstrated by micromagnetic simulations. By analogy to the fields of photonics, we first establish magnonic Snell’s law for spin waves passing through an interface between two media with different dispersion relations due to different Dzyaloshinskii–Moriya interactions. Based on magnonic Snell’s law, we find that spin waves can experience total internal reflection. The critical angle of total internal reflection is strongly dependent on the sign and strength of Dzyaloshinskii–Moriya interaction. Furthermore, spin-wave beam fiber and spin-wave lens are designed by utilizing the artificial magnonic metamaterials with inhomogeneous Dzyaloshinskii–Moriya interactions. Our findings open up a rich field of spin waves manipulation for prospective applications in magnonics.

Keywords: Spin waves; Dzyaloshinskii–Moriya interaction; Ferromagnetism; Spintronics

1. Introduction

Magnonics (or magnon spintronics) is an emerging field concentrating on the generation, detection, and manipulation of magnons, the quanta of spin-wave, in ferromagnetic or antiferromagnetic metals and insulators [1–9]. Because spin waves in magnetic insulators exhibit both low energy dissipation and long coherence length, it constitutes a competitive alternative to electronic devices and is deemed as a promising candidate for high-quality information carrier [10–12]. Over the past decades, many properties of the spin waves have been demonstrated experimentally, in analogy with electromagnetic waves: excitation and propagation [13–16], reflection and refraction [17–20], interference and diffraction [21–23], tunnelling and Doppler effect [24–26]. So far, based on recent progress in the fabrication of magnetic nanostructures, various device concepts have been proposed such as the spin-wave logic gates and circuits [10,27,28], waveguides [29,30], multiplexors [31], splitter [32] and diodes [33]. The implementations of those devices is usually achieved by the application of external local magnetic fields [24], spin current [26,34] or magnetic textures (for example, the chiral domain wall) [27,29,35] to control the dispersion relation of spin waves, thereby steering the spin-wave propagation properties. Despite the soundness of the concepts, however, there are some inherent drawbacks and obstacles to applications. Firstly, generating a local high-frequency magnetic field on micro-sized devices complicates the structure design and the local field is often spatially inhomogeneous, which can inhibit the benefits of the device [36]. In addition, unstable magnetic textures under external excitation and at room temperature may give rise to poor reliability and high bit error rates. Therefore, it is desirable to find a new method to manipulate the propagation of spin waves.

Citation: Zhuo, F.; Li, H.; Cheng, Z.; Manchon, A. Magnonic Metamaterials for Spin-Wave Control with Inhomogeneous Dzyaloshinskii–Moriya Interactions. *Journal Not Specified* **2022**, *1*, 0. <https://doi.org/>

Received:

Accepted:

Published:

Publisher’s Note: MDPI stays neutral with regard to jurisdictional claims in published maps and institutional affiliations.

Copyright: © 2022 by the authors. Submitted to *Journal Not Specified* for possible open access publication under the terms and conditions of the Creative Commons Attribution (CC BY) license (<https://creativecommons.org/licenses/by/4.0/>).

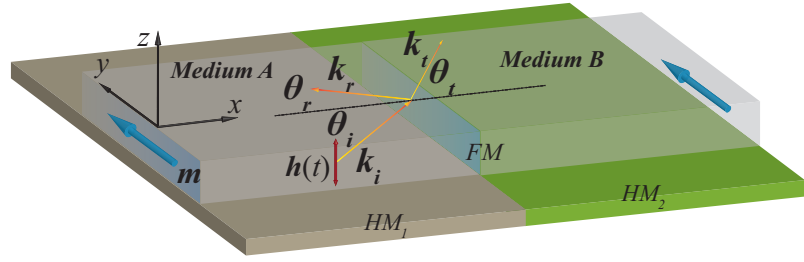


Figure 1. Schematic illustration of spin-wave transmission and reflection at an interface between media A and B with different interfacial DMI in a thin YIG film. The interfacial DMI step here is realized by utilizing two different HM layers (HM_1 and HM_2) below the YIG film. The blue arrows along \hat{y} direction denote the magnetization \mathbf{m} . \mathbf{k}_i , \mathbf{k}_t and \mathbf{k}_r are the wave vectors of the incident, refracted and reflected spin-wave shown as the yellow red arrows, respectively. $\theta_{i,t,r}$ denote their angles with respect to the interface normal. The red double-headed arrow shows the Gaussian distribution AC Magnetic field $\mathbf{h}(t)$ exciting the spin-wave.

Recent discoveries in graded-index magnonics or magnonic metamaterials provide a new way to manipulate spin-wave propagation [37,38], which is inspired by the fields of graded-index photonics (or photonic metamaterials) [39–41]. The core idea of graded-index magnonics is to manipulate spin-wave propagation by designing spatially varied magnonic refractive index. In magnetic thin films with in-plane magnetization, the spin-wave dispersion relation described by the Landau-Lifshitz-Gilbert (LLG) equation exhibits a much more complex structure compared to the isotropic dispersion relation of light. This offers extremely rich opportunities to modulate magnonic refractive index. Up to now, it has been shown that the graded magnonic refractive index can be created by modification of materials properties, such as non-uniform saturation magnetization or exchange constant [42–44], the magnetic anisotropy [17,18], or the internal magnetic field [35,45]. It can be also achieved by utilizing non-uniform external magnetic field [37,46–48], electric field (voltage) [49,50], or temperature [51,52]. Therefore, graded-index magnonics is expected to overcome the current limitation of magnonics and pave feasible routes for the implementation of spin-wave devices.

In this paper, we theoretically propose a magnonic metamaterial, in which we modulate the refractive index of spin waves with inhomogeneous Dzyaloshinskii-Moriya interaction (DMI) to avoid hardly controllable local magnetic field and unstable magnetic textures. The DMI is an antisymmetric exchange interaction arising from the lack of structural inversion symmetry in magnetic films [53,54]. It has been found both for bulk materials [55–57] and magnetic interfaces [58]. Here, we focus on a spatial inhomogeneous interfacial DMI present in ferromagnet/heavy metal (FM/HM) bilayers realized by tuning the thickness of ferromagnetic layer or HM layer [59–61], the degree of hybridization between 3d-5d states [62], or utilizing a local gating [63]. We begin our work by rapidly deriving the spin-wave dispersion relation with spatially modulated DMI. Then, we further study spin-wave refraction and reflection at the interface between two magnetic media with different DMI and build the generalized Snell’s law of spin waves, similar to Snell’s law in optics. According to the magnonic Snell’s law, spin-wave can also experience total internal reflection (TIR) at the DMI step interface when their incident angle is larger than a critical value (i.e., critical angle). Moreover, magnonic Snell’s law and TIR are observed and confirmed by micromagnetic simulations. Utilizing the artificial magnonic metamaterials based on spatially modulated DMI, a spin-wave fiber owing to TIR which can transmit spin waves over a long distance, and a spin-wave lens holding tremendous possibility to build spin-wave circuits are proposed as proofs of concept.

The paper is organized as follows. In Sec. 2 we introduce our theoretical model and method. Detailed results of micromagnetic simulations are presented in Sec. 3. Then, we discuss the realization of spin-wave fibers and lenses in Sec. 4. Finally, we end the paper with a summary in Sec. 5.

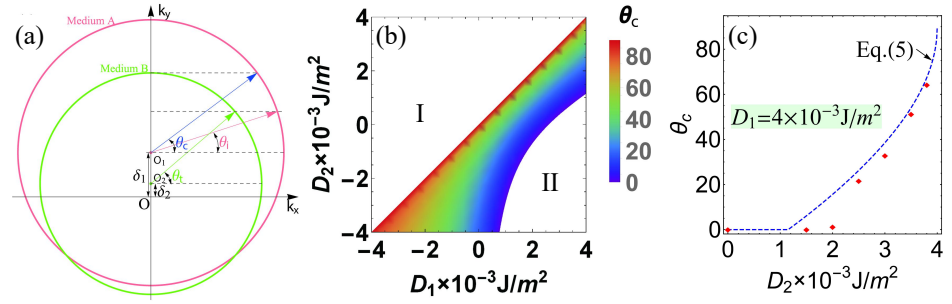


Figure 2. (a) Schematic illustrations of reflection and refraction of spin-wave at an interface between two different media in wave vector $(k_x - k_y)$ space. The pink and green circles indicate the individual frequency contours of the allowed modes in the same-color-coded media A and B, respectively. The color-coded arrows denote the spin-wave vectors \mathbf{k} propagating in each medium, as indicated by the incident (pink) and refracted (green) rays. The blue arrow denotes the critical angle. (b) Phase diagrams of critical angle θ_C in the $D_1 - D_2$ plane. No TIR exists in white regions. (c) Critical angle θ_c as a function of DMI constants D_2 with a fixed DMI constant $D_1 = 4 \times 10^{-3} \text{ J/m}^2$. The symbols (red squares) are simulation data, and solid curve is analytical results of Eq (5).

2. Analytical model

2.1. Magnonic Snell's law

We consider a thin magnetic film in the $x - y$ plane with the thickness much smaller than lateral dimensions of the film ($L_z \ll L_x, L_y$), whose initial magnetization is homogeneous along $\hat{\mathbf{y}}$ direction. The magnetization dynamics is governed by the LLG equation [64],

$$\frac{\partial \mathbf{m}}{\partial t} = -\frac{\gamma}{M_s} \mathbf{m} \times \mathbf{H}_{eff} + \alpha \mathbf{m} \times \frac{\partial \mathbf{m}}{\partial t}, \quad (1)$$

where \mathbf{m} is the unit direction of local magnetization $\mathbf{M} = M_s \mathbf{m}$ with a saturation magnetization M_s . α is the phenomenological Gilbert damping constant and γ is the gyromagnetic ratio. Here, $\mathbf{H}_{eff} = A^* \nabla^2 \mathbf{m} - D^*(x) (\hat{\mathbf{z}} \times \nabla) \times \mathbf{m} - K^* m_y \hat{\mathbf{y}}$ is the effective field [65], and $A^* = 2A/\mu_0 M_s$, $D^*(x) = 2D(x)/\mu_0 M_s$, $K^* = 2K/\mu_0 M_s$, respectively. A is the symmetric exchange constant, $D(x)$ is the interfacial antisymmetric DMI constant spatially inhomogeneous along the x direction, K is the in-plane anisotropy and μ_0 is the permeability of vacuum. Under the perturbative approximation, the small-amplitude spin waves propagating in the $x - y$ plane takes the following form [66]:

$$\mathbf{m} = \hat{\mathbf{y}} + \delta \mathbf{m} \exp [i(\hat{\mathbf{k}} \cdot \hat{\mathbf{r}} - \omega t)], \quad (2)$$

where $\delta \mathbf{m} = (\delta m_x, 0, \delta m_z)$ is the spin-wave contribution to magnetization ($|\delta \mathbf{m}| \ll 1$). $\delta \mathbf{k} = (k_x, k_y, 0)$ is the spin-wave wavevector. Considering the system shown in Fig. 1, we use a DMI step (i.e., $D = D_1$ in medium A and $D = D_2$ in medium B) to induce a difference in spin-wave dispersion relations between two magnetic domains. Inserting Eq. (2) into Eq. (1) and neglecting higher order terms, we obtain the spin-wave dispersion relation in each region [67,68],

$$\omega(\mathbf{k}_n) = \gamma \mu_0 (K^* + A^* k_n^2 - D_n^* k_{n,y}), \quad (3)$$

with $D_n^* = 2D_n/\mu_0 M_s$ and $k_n = \sqrt{k_{n,x}^2 + k_{n,y}^2}$. The spin-wave group velocity is $\mathbf{v}_{g,n} = \partial \omega / \partial \mathbf{k}_n = 2A^* \mathbf{k}_{g,n}$, where $\mathbf{k}_{g,n} = \mathbf{k}_n - \delta_n \hat{\mathbf{y}}$ and $\delta_n = D_n^*/2A^*$. To simplify the model, we assume that the group velocity is parallel to the phase velocity at each point of the dispersion relation, that is to say, the dispersion relation is isotropic. Eq. (3) represents an isofrequency circle with radius $k_{g,n}$ in momentum space, whose center deviates from the origin by δ_n in $-\hat{\mathbf{y}}$ direction as illustrated in Fig. 2(a). Nevertheless, in the magnetic films with in-plane magnetizations, the spin-wave dispersion relation is anisotropic at low frequencies, where dipolar contribution dominates. When increasing frequency, the isofrequency contours smoothly transform through elliptical to almost circular. Consequently, the dispersion

relation is isotropic determined by the exchange interactions at high frequencies. In the following simulations, we use quite high frequency spin waves (100 GHz), so the spin-wave dynamic is determined by the exchange interactions.

Based on translation symmetry considerations, the refraction angle obeys the generalized Snell's law which guarantees continuity of tangential components of the \mathbf{k} vector across the DMI step interface along the \hat{y} axis, such that $k_{i,y} = k_{t,y}$ [17,18,35]. Consequently, the generalized magnonic Snell's law based on modifying the dispersion relation with inhomogeneous DMI can be rewritten in the following form:

$$k_{g,i} \sin \theta_i + \delta_i = k_{g,t} \sin \theta_t + \delta_t, \quad (4)$$

where $k_{g,n} = \sqrt{(\omega/\gamma\mu_0 - K^*)/A^* + \delta_n^2}$ is the value of $\mathbf{k}_{g,n}$. Here the generalized Snell's law shown in Eq. (4) is derived for an interface between two spin-wave media with different material parameters (interfacial DMI), which can be viewed as graded-index magnonic metamaterials. However, it is different from the Snell's laws based on the interface inside magnetic textures, such as chiral domain walls (the interface formed by two opposite magnetic domains) [35].

2.2. Total internal reflection

Analogously to the case of electromagnetic waves in photonics or acoustic waves in phononics, spin waves are also expected to be completely reflected by the interface when spin-wave travels from a *denser* medium with a higher refractive index to a *thinner* medium with a lower refractive index known as TIR. TIR occurs when the incident angle $\theta_i \geq \theta_c$, where θ_c is often called critical angle. When $\theta_i = \theta_c$ refracted spin-wave travels along the interface between the two media or the angle of refraction θ_t is $\pi/2$. According to the magnonic Snell's law in Eq. (4), the critical angle can be expressed as

$$\theta_c = \arcsin\left(\frac{k_{g,t} - \delta_t}{k_{g,i}}\right), \quad (5)$$

where $\delta = \delta_i - \delta_t$. Specially, Eq. (5) shows that θ_c equals $\pi/2$ when the DMI is homogenous ($D_1 = D_2$), i.e., all incident spin waves are fully transmitted and no reflection occurs. Furthermore, when δ (the difference between DMI in two regions) is chosen to be large enough, a gap falls in between the two isofrequency circles and TIR occurs at all incident angles (i.e., $\theta_c = 0$). Equations (4) and (5) are the main analytical results in our paper.

3. Micromagnetic simulations

To test the validity of these analytical findings in realistic situations, micromagnetic simulations have been proved to be an efficient tool for the investigation of spin-wave dynamics in various magnetic textures and geometries. The simulations here are performed in the GPU-accelerated micromagnetic simulations program MuMax3 [69] which solves time-dependent LLG Eq. (1) based on the finite difference method. In our simulations, we used typical magnetic parameters for YIG at zero temperature [70]: $M_s = 0.194 \times 10^5$ A/m, $A = 3.8$ pJ/m and $K = 10^4$ J/m³. All simulations presented here were performed for a thin film of size $L_x \times L_y \times L_z$ which discretized with cuboid meshes of dimensions $l_x \times l_y \times l_z$. The lateral dimensions of unit mesh (l_x and l_y) and the thickness of the film L_z are all smaller than the exchange length of YIG [3]. The simulations have been implemented with the mesh size $2 \times 2 \times 2$ nm³. The simulations were split up into two stages, static and dynamic stage. In the first stage, the static stage, the magnetic configuration is stabilized by minimization of the total energy starting from the random magnetic configuration with high value of damping ($\alpha = 0.5$). In the dynamic stage of the simulations, the equilibrium magnetic configuration was used to excite a spin-wave beam that propagates through the film with a small damping parameter ($\alpha = 0.0005$) to ensure long-distance propagation. During this step, a Gaussian type spin-wave beam was continuously generated by a harmonic dynamic external magnetic field following Gaussian distribution function in a small rectangular

region (red double-headed arrow shown in Fig. 1). The detailed description of the Gaussian spin-wave beam generation procedure can be found in Ref. [72]. The Gaussian spin-wave beam is clearly visible and does not change with time after exciting continuously a sufficiently long time, which corresponding to a steady spin-wave propagation. Moreover, to avoid spin-wave reflection at the boundaries of the film, absorbing boundary condition is applied on all boundaries by assigning a large damping constant ($\alpha = 1$) near the edges.

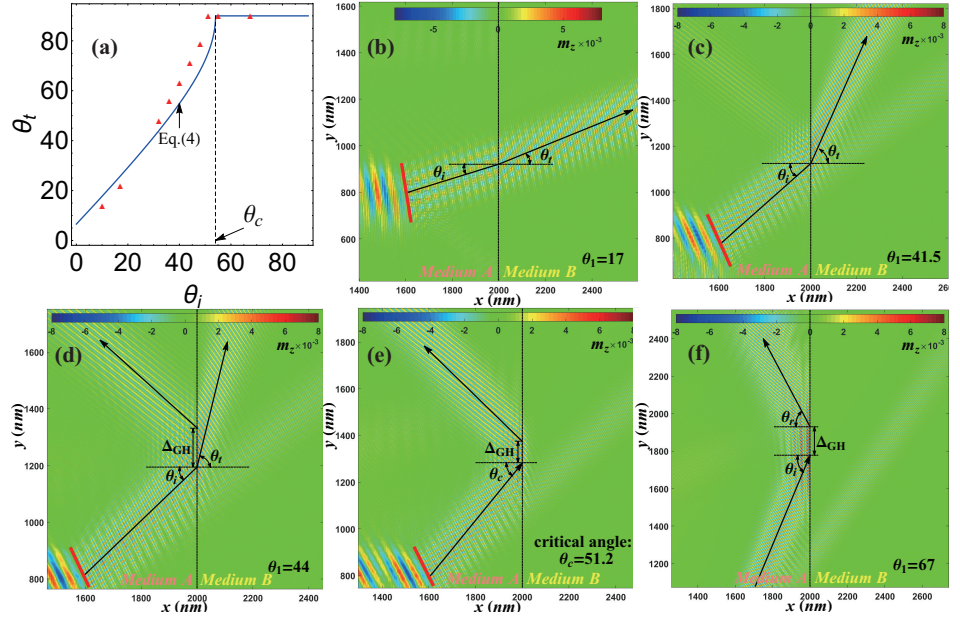


Figure 3. (a) The refracted angle as a function of the incident angle. Vertical dashed and solid line corresponds to critical angle θ_c . (b)-(f) The micromagnetic simulations results for spin-wave beams reflection and refraction under different incident angle (b) $\theta_i = 17^\circ$, (c) $\theta_i = 41.5^\circ$, (d) $\theta_i = 44^\circ$, (e) $\theta_i = 51.2^\circ$ and (f) $\theta_i = 67^\circ$. The DMI constants in medium A and B are $D_1 = 4 \times 10^{-3} \text{J/m}^2$ and $D_2 = 3.5 \times 10^{-3} \text{J/m}^2$, respectively. The color map shows z component of the magnetization in the snapshot of micromagnetic simulations at some selected time. The black solid lines correspond to the rays of the incident and refractive beams. The red rectangular area is the excitation area of spin-wave and the exciting field frequency is $f = 100$ GHz.

In order to verify the magnonic Snell's law in Eq. (4) for the spin-wave propagation through a DMI step interface, we focus on a $4 \mu\text{m} \times 4 \mu\text{m} \times 2 \text{nm}$ nanowire. The spin-wave beams presented here are all exchange-dominated spin waves with 200 nm beam width and 30 nm wavelength generated by a external AC magnetic field with frequency $f = 100$ GHz. The phase diagram of the critical angle θ_c in the $D_1 - D_2$ plane is shown in Fig. 2(b). As $D_1 < D_2$ in white region I, spin waves transmit from a thinner medium with a lower refractive index to a denser medium with a higher refractive index, thus no TIR happens. A gap falls in between the two isofrequency circles, in other words TIR occurs in all incident angles when δ is chosen to be large enough as shown in white region II. Fig. 2(c) shows the critical angle as a function of the DMI constant D_2 in medium B, where the DMI constant of medium A is fixed at $D_1 = 4 \times 10^{-3} \text{J/m}^2$. All incident angle spin waves are totally reflected at a small D_2 corresponding to Region II in Fig. 2(b). After that, the critical angle increases monotonically with D_2 and shows a good agreement with the analytical results.

In Fig. 3(a) we show the refracted angle θ_t as a function of the incident angle θ_i from micromagnetic simulations (red triangle) and the prediction from Eq. (4) (blue curve) with DMI constants $D_1 = 4 \times 10^{-3} \text{J/m}^2$ and $D_2 = 3.5 \times 10^{-3} \text{J/m}^2$, respectively. The micromagnetic simulation for the five different incident angles, $\theta_i = 17^\circ$, 41.5° , 44° , 51.2° and 67° , are displayed in Figures 3 (b)-(f). Figures 3(b)-(d) correspond to refraction mode, Figures 3(e) and 3(f) are total reflection mode, respectively. Vertical dashed lines correspond to the interface at $x = 2000$ nm between medium A (left) and medium B (right).

The critical angle observed in our simulation is estimated to be $\theta_c = 51.2^\circ$ as shown in Fig. 3(e). It is important to comment that spin-wave propagation direction is not strictly perpendicular to spin-wave wavefronts in our simulation. That is to say, it is easy to observe strong anisotropy in the propagation of spin waves. Typically, for in-plane magnetized films, spin waves dynamics is anisotropic. It means that iso-frequency dispersion relation lines (IFDRLs, slices of dispersion relation for particular frequencies) are not circular. Therefore, the group velocity and phase velocities (parallel to the wave-vector) are not parallel to each other, since the group velocity direction should be normal to the IFDRLs [71]. Such an intrinsic anisotropy called spin-wave collimation effect is common in ferromagnetic films with the magnetization fixed in the plane of the film by an external magnetic field or a strong in-plane anisotropy [72]. However, in the present case the symmetry of the spin-wave dispersion relation is broken due to the presence of DMI and the wave vector can be shifted from the direction perpendicular to spin-wave wavefronts [66]. This anisotropy decreases with increasing frequency of spin-wave but it is still present at high frequency $f = 100$ GHz assumed in our simulations. Moreover, a lateral shift Δ_{GH} of the spin-wave beam is observed at the interface between the reflected and the incident beams, which is called the Goos-Hünchen (GH) effect. The GH effect for spin-wave was reported in Refs. [71,72]. Furthermore, detailed investigations elucidating the role of inhomogeneous DMI on the GH shift in the reflection of spin-wave at the interface have been discussed in Ref. [20].

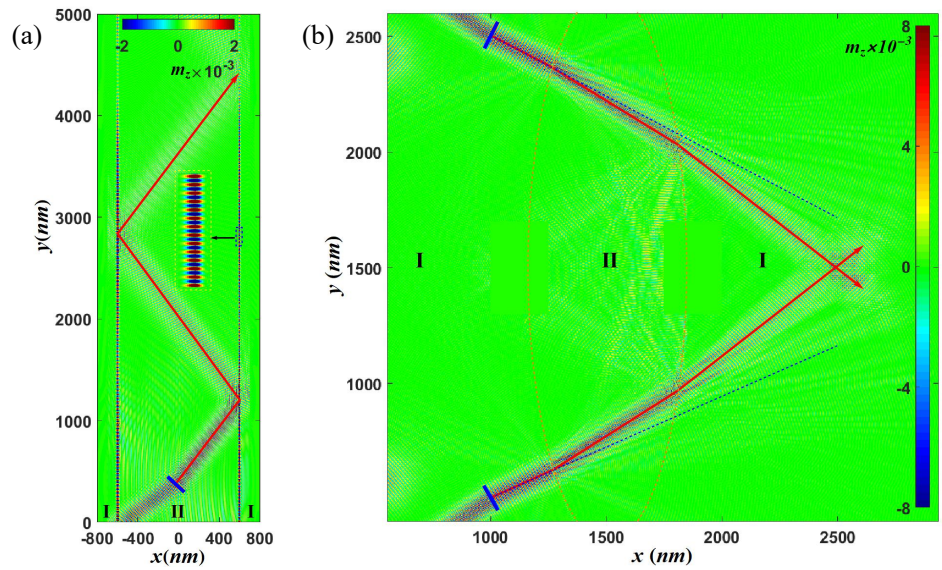


Figure 4. (a) Schematic illustration of a spin-wave fiber. The inset shows the enlarged figure at the interface. (b) schematic illustration of a spin-wave convex lens. In all of the above figures, the color map shows z component of the magnetization in the snapshot of micromagnetic simulations at some selected time. The spin-wave trajectories are represented by solid red lines with an arrow. The simulated propagation of the spin wave excited by a AC source in blue bars with an exciting frequency $f = 100$ GHz.

4. Spin-wave fiber and lens

We now turn to the realization of the spin-wave fiber and spin-wave lens, which are important to manipulate spin waves in spin-wave circuitry. Two kinds of spin-wave fiber have been proposed and designed, one based on the TIR by the magnetic domain wall [35] and the other based on the TIR in the medium with uniform external magnetic field [48]. Here utilizing the TIR at the interface with a DMI step, we propose a new type spin-wave fiber as shown in Fig. 4(a) of system size $12 \mu\text{m} \times 1.6 \mu\text{m} \times 2 \text{nm}$. The DMI constant in the core (region II, $|x| \leq 400 \text{nm}$) is $0.5 \times 10^{-3} \text{J/m}^2$ surrounded by transparent cladding FM layers (region I, $|x| \geq 400 \text{nm}$) with a lower index of refraction ($D = -0.4 \times 10^{-3} \text{J/m}^2$).

Two DMI steps are formed with the critical angle $\theta_c = 48^\circ$. The upper one is located at $x = -400$ nm and the lower one is located at $x = 400$ nm. In Fig. 4(a), the spin-wave beam born at the middle of the nanowire (blue bar) propagates inside the core with an incident angle of 52° greater than θ_c . It is different from the unidirectional spin-wave fiber based on domain walls [35]. The fiber here is fully bidirectional for both right/left-moving spin-wave beams when the incident angle is greater than the critical angle. More interestingly, a bound spin-wave mode propagates a long distance inside the DMI step interface as illustrated in the inset of Fig. 4(a). Similar to the bound spin wave mode inside a domain wall which acts as a local potential well for spin waves [29,73], a DMI step also creates an imaginary potential well for bound spin wave mode [74]. The details will be discussed in our future publications.

A fundamental building block in spin-wave circuitry is a spin-wave lens that can focus or diverge spin-wave beams. Since the dispersion relation strongly depends on DMI constant, we propose a spin-wave lens by tuning DMI distribution in the film. Fig. 4(b) illustrates an example of spin-wave convex lens (region I inside red dotted lines) with DMI constant inside/outside the lens $D = 0.5/ -0.4 \times 10^{-3} \text{J/m}^2$, respectively. The size of the sample presented here is $6 \mu\text{m} \times 6 \mu\text{m} \times 2$ nm. Comparing the solid blue lines along the incident spin-wave beam propagation direction and the spin-wave trajectory (solid red lines with an arrow) passing through the lens, it is easy to observe focussing in the propagation of spin waves. Furthermore, a concave spin-wave lens can be obtained by reversing the DMI constants of regions I and II, which can be used to spit the spin-wave beams. Consequently, we believe that the inhomogeneous DMI can be a good playground to study spin-wave beam propagation [75].

5. Conclusion

In conclusion, we theoretically and numerically studied spin-wave beam propagation in a two-dimensional ferromagnetic film with an inhomogeneous interfacial DMI. Utilizing spatially varied magnonic refractive index introduced by the variation of DMI, a magnonic metamaterial or graded-index magnonic material can be realized. Snell's law and TIR for spin waves were predicted with a DMI step interface. Moreover, spin-wave fibers and spin-wave lenses are designed and studied by micromagnetic simulations. We believe that our findings shall open up alternative direction for building reconfigurable, stabilized and scalable spin-wave circuitry in magnon spintronics devices.

However, the parameters we adopted in our simulations to investigate spin wave propagation in the presence of spatially modulated DMI are not meant to represent a specific material but rather to explore the physical conditions under which the spin-wave total reflection occurs. From the materials standpoint, we acknowledge that the dual requirement of low damping and large DMI may seem incompatible since spin-orbit coupling originating from the adjacent heavy metal layer is detrimental to the former but central to the latter. The excitation of short-wavelength propagating spin waves with wavelength 45 nm in a YIG thin film covered by $\text{Co}_{25}\text{Fe}_{75}$ nanowires was reported in a recent experiment [76], where the effective damping was only enhanced to about 10^{-3} . Meanwhile, recent progress in materials science has proven that certain magnetic insulators do possess sizable DMI either in their bulk [77–79] or at the interface [80–82]. Although these values remain small (typically $\sim 10^{-3} - 10^{-2} \text{mJ/m}^2$), these results open interesting perspectives for the achievement of large DMI in magnetic insulators.

Author Contributions: Conceptualization, F.Z. and A.M.; methodology, F.Z.; software, F.Z.; validation, F.Z. and A.M.; formal analysis, F.Z., H.L. Z.C. and A.M.; investigation, F.Z.; resources, H.L. and A.M.; data curation, F.Z.; writing—original draft preparation, F.Z.; writing—review and editing, H.L., Z.C. and A.M.; visualization, H.L., Z.C. and A.M.; supervision, A.M.; project administration, A.M.; funding acquisition, H.L., Z.C. and A.M. All authors have read and agreed to the published version of the manuscript.

Funding: F.Z. and H.L. acknowledge the support from National Key R&D Program of China (No. 2018YFB0407600), Henan University (No. CJ3050A0240050) and National Natural Science Foundation of China (No. 11804078). F.Z. was supported by King Abdullah University of Science and Technology (KAUST). A.M. acknowledges support from the Excellence Initiative of Aix-Marseille Université—A*Midex, a French "Investissements d’Avenir" program. Z.C. acknowledges the support from Grant No. ARC (DP190100150).

Data Availability Statement: The data that support the findings of this study are available upon reasonable request from the authors.

Conflicts of Interest: The authors declare no conflict of interest.

References

1. Kruglyak, V.V.; Hicken R.J. Magnonics: Experiment to prove the concept. *J. Magn. Magn. Mater.* **2006**, *306*, 191. 234
2. Kruglyak, V.V.; Demokritov, S.O.; Grundler, D. Magnonics. *J. Phys. D: Appl. Phys.* **2010**, *43*, 264001. 235
3. Serga, A.A.; Chumak, A.V.; Hillebrands, B. YIG magnonics. *J. Phys. D: Appl. Phys.* **2010**, *43*, 264002. 236
4. Lenk, B.; Ulrichs, H.; Garbs, F.; Münzenberg, M. The Building Blocks of Magnonics. *Phys. Rep.* **2011**, *507*, 107. 237
5. Demokritov, S.O.; Slavin, A.N. *Magnonics: From Fundamentals to Applications*. 1st ed.; Springer: New York, US, 2013; pp. 125. 238
6. Chumak, A.V.; Vasyuchka, V.I.; Serga, A.A.; Hillebrands, B. Magnon spintronics. *Nat. Phys.* **2015**, *11*, 453. 239
7. Baltz, V.; Manchon, A.; Tsoi, M.; Moriyama, T.; Ono, T.; Tserkovnyak, Y. Antiferromagnetic spintronics. *Rev. Mod. Phys.* **2018**, *90*, 015005. 240
8. Barman, A. *et. al.* The 2021 Magnonics Roadmap. *J. Phys.: Condens. Matter* **2021**, *33*, 413001. 242
9. Bonbien, V.; Zhuo, F.; Salimath, A.; Ly, O.; About, A.; Manchon, A. Topological aspects of antiferromagnets. *J. Phys. D: Appl. Phys.* **2022**, *55*, 103002. 243
10. Khitun, A.; Bao, M.; Wang, K.L. Magnonic logic circuits. *J. Phys. D: Appl. Phys.* **2010**, *43*, 264005. 245
11. Chumak, A.V.; Serga, A.A.; Hillebrands, B. Magnon transistor for all-magnon data processing. *Nat. Commun.* **2014**, *5*, 4700. 246
12. Zhuo, F.; Li, H.; Manchon, A. Topological phase transition and thermal Hall effect in kagome ferromagnets. *Phys. Rev. B* **2021**, *104*, 144422; Topological thermal Hall effect and magnonic edge states in kagome ferromagnets with bond anisotropy. *New J. Phys.* **2022**, *24*, 023033. 247
13. Liu, Z.; Giesen, F.; Zhu, X.; Sydora, R.D.; Freeman, M.R. Spin Wave Dynamics and the Determination of Intrinsic Damping in Locally Excited Permalloy Thin Films. *Phys. Rev. Lett.* **2007**, *98*, 087201. 250
14. Serga, A.A.; Demokritov, S.O.; Hillebrands, B.; Slavin, A.N. Self-Generation of Two-Dimensional Spin-Wave Bullets. *Phys. Rev. Lett.* **2014**, *92*, 117203. 251
15. Covington, M.; Crawford, T.M.; Parker, G.J. Time-Resolved Measurement of Propagating Spin Waves in Ferromagnetic Thin Films. *Phys. Rev. Lett.* **2002**, *89*, 237202. 254
16. Demidov, V.E.; Jersch, J.; Demokritov, S.O.; Rott, K.; Krzysteczko, P.; Reiss, G. Transformation of propagating spin-wave modes in microscopic waveguides with variable width. *Phys. Rev. B* **2009**, *79*, 054417; Demidov, V.E.; Kostylev, M.P.; Rott K.; Münchenberger, J.; Reiss, G.; Demokritov, S.O. Excitation of short-wavelength spin waves in magnonic waveguides. *Appl. Phys. Lett.* **2011**, *99*, 082507. 256
17. Stigloher, J. Snell’s Law for Spin Waves. *Phys. Rev. Lett.* **2016**, *117*, 037204. 260
18. Kim, S.K.; Choi, S.; Lee, K.S.; Han, D.S.; Jung, D.E.; Choi, Y.S. Negative refraction of dipole-exchange spin waves through a magnetic twin interface in restricted geometry. *Appl. Phys. Lett.* **2008**, *92*, 212501. 261
19. Wang, Z.; Zhang, B.; Cao, Y.; Yan, P. Probing the Dzyaloshinskii-Moriya Interaction via the Propagation of Spin Waves in Ferromagnetic Thin Films. *Phys. Rev. Applied* **2018**, *10*, 054018. 263
20. Wang, Z.; Cao, Y.; Yan, P. Goos-Hänchen effect of spin waves at heterochiral interfaces. *Phys. Rev. B* **2019**, *100*, 064421. 265
21. Choi, S.K.; Lee, K.S.; Kim, S.K. Spin-wave interference. *Appl. Phys. Lett.* **2006**, *89*, 062501. 266
22. Perzlmaier, K.; Woltersdorf, G.; Back, C.H. Observation of the propagation and interference of spin waves in ferromagnetic thin films. *Phys. Rev. B* **2008**, *77*, 054425. 267
23. Birt, D. R.; Gorman, B.O.; Tsoi, M.; Li, X.; Demidov, V.E.; Demokritov, S.O. Diffraction of spin waves from a submicrometer-size defect in a microwaveguide. *Appl. Phys. Lett.* **2009**, *95*, 122510. 269
24. Demokritov, S.O.; Serga, A.A.; André, A.; Demidov, V.E.; Kostylev, M.P.; Hillebrands, B.; Slavin, A.N. Tunneling of Dipolar Spin Waves through a Region of Inhomogeneous Magnetic Field. *Phys. Rev. Lett.* **2004**, *93*, 047201. 271
25. Stancil, D.D.; Henty, B.E.; Cepni, A.G.; Van’t Hof, J.P. Observation of an inverse Doppler shift from left-handed dipolar spin waves. *Phys. Rev. B* **2006**, *74*, 060404. 273
26. Vlaminck, V.; Bailleul, M. Current-Induced Spin-Wave Doppler Shift. *Science* **2008**, *322*, 410. 274
27. Hertel, R.; Wulfhekel, W.; Kirschner, J. Domain-Wall Induced Phase Shifts in Spin Waves. *Phys. Rev. Lett.* **2004**, *93*, 257202. 276
28. Lee, K.S.; Kim, S.K. Conceptual design of spin wave logic gates based on a Mach-Zehnder-type spin wave interferometer for universal logic functions. *J. Appl. Phys.* **2008**, *104*, 053909. 277
29. Sanchez, F.G.; Borys, P.; Soucaille, R.; Adam, J.P.; Stamps, R.L.; Kim, J.V. Narrow Magnonic Waveguides Based on Domain Walls. *Phys. Rev. Lett.* **2015**, *114*, 247206. 279

30. Mulkers, J.; Waeyenberge, B.V.; Milošević, M.V. Effects of spatially engineered Dzyaloshinskii-Moriya interaction in ferromagnetic films. *Phys. Rev. B* **2017**, *95*, 144401. 281
31. Vogt, K.; Fradin, F. Y.; Pearson, J.E.; Sebastian, T.; Bader, S.D.; Hillebrands, B.; Hoffmann, A.; Schultheiss, H. Realization of a spin-wave multiplexer. *Nat. Commun.* **2014**, *5*, 3727. 282
32. Sadovnikov, A.V.; Davies, C.S.; Grishin, S.V.; Kruglyak, V.V.; Romanenko, D.V.; Sharaevskii, Y.P.; Nikitov, S.A. Magnonic beam splitter: The building block of parallel magnonic circuitry. *Appl. Phys. Lett.* **2015**, *106*, 192406. 283
33. Lan, J.; Yu, W.; Wu, R.; Xiao, J. Spin-Wave Diode. *Phys. Rev. X* **2015**, *5*, 041049. 284
34. Seo, S.M.; Lee, K.J.; Yang, H.; Ono, T. Current-Induced Control of Spin-Wave Attenuation. *Phys. Rev. Lett.* **2009**, *102*, 147202. 285
35. Yu, W.; Lan, J.; Wu, R.; Xiao, J. Magnetic Snell's law and spin-wave fiber with Dzyaloshinskii-Moriya interaction. *Phys. Rev. B* **2016**, *94*, 140410. 286
36. Jamali, M.; Kwon, J. H.; Seo, S.M.; Lee, K.J.; Yang, H. Spin wave nonreciprocity for logic device applications. *Sci. Rep.* **2013**, *3*, 3160. 287
37. Davies, C.S. *et al.* Towards graded-index magnonics: Steering spin waves in magnonic networks. *Phys. Rev. B* **2015**, *92*, 020408(R). 288
38. Davies, C.S.; Kruglyak, V.V. Graded-index magnonics. *Low Temp. Phys.* **2015**, *41*, 760. 289
39. Marchand, E. W. *Gradient Index Optics*. 1st ed.; ScienceDirect: London, UK, 1978; pp. 125. 290
40. Chen, H.; Chan, C.T.; Sheng, P. Transformation optics and metamaterials. *Nat. Mater.* **2010**, *9*, 387. 291
41. Pendry, J.B.; Domínguez, A.I.F.; Luo, Y.; Zhao, R. Capturing photons with transformation optics. *Nat. Phys.* **2013**, *9*, 518. 292
42. Dadoenkova, Y.S.; Dadoenkova, N.N.; Lyubchanskii, I.L.; Sokolovskyy, M.L.; Kłos, J.W.; Romero-Vivas, J.; Krawczyk, M. Huge Goos-Hänchen effect for spin waves: A promising tool for study magnetic properties at interfaces. *Appl. Phys. Lett.* **2012**, *101*, 042404. 293
43. Xi, H.; Xue, S. Spin-wave propagation and transmission along magnetic nanowires in long wavelength regime. *J. Appl. Phys.* **2007**, *101*, 123905.; Xi, H.; Wang, X.; Zheng, Y.; Ryan, P.J. Spin wave propagation and coupling in magnonic waveguides. *J. Appl. Phys.* **2008**, *104*, 063921. 294
44. Vogel, M.; Aßmann, R.; Pirro, P.; Chumak, A.V.; Hillebrands, B.; Freymann, G.V. Control of Spin-Wave Propagation using Magnetisation Gradients. *Sci. Rep.* **2018**, *8*, 11099. 295
45. Xing, X.; Zhou Y. Fiber optics for spin waves. *NPG Asia Mater.* **2016**, *8*, e246. 296
46. Perez, N.; Diaz, L.L. Magnetic field induced spin-wave energy focusing. *Phys. Rev. B* **2015**, *92*, 014408. 297
47. Houshang, A.; Iacocca, E.; Dürrenfeld, P.; Sani, S.; Akerman, J.; Dumas, R. Spin-wave-beam driven synchronization of nanocontact spin-torque oscillators. *Nat. Nanotechnol.* **2016**, *11*, 280. 298
48. Gruszecki, P.; Krawczyk, M. Spin wave beam propagation in ferromagnetic thin film with graded refractive index: mirage effect and prospective applications. *Phys. Rev. B* **2018**, *97*, 094424. 299
49. Wang, S.; Guan, X.; Cheng, X.; Lian, C.; Huang, T.; Miao, X. Spin-wave propagation steered by electric field modulated exchange interaction. *Sci. Rep.* **2016**, *6*, 31783. 300
50. Kakizakai, H.; Yamada, K.; Ando, F.; Kawaguchi, M.; Koyama, T.; Kim, S.; Moriyama, T.; Chiba, D.; Ono, T. Influence of sloped electric field on magnetic-field-induced domain wall creep in a perpendicularly magnetized Co wire. *Jpn. J. Appl. Phys.* **2017**, *56*, 050305. 301
51. Vogel, M.; Chumak, A.V.; Waller E.H.; Langner, T.; Vasyuchka, V.I.; Hillebrands, B.; Freymann, G.V. Optically reconfigurable magnetic materials. *Nat. Phys.* **2015**, *11*, 487. 302
52. Busse, F.; Mansurova, M.; Lenk, B.; Ehe, M.; Münzenberg, M. A scenario for magnonic spin-wave traps. *Sci. Rep.* **2015**, *5*, 12824. 303
53. Dzyaloshinskii, I.E. A thermodynamic theory of "weak"ferromagnetism of antiferromagnetics. *J. Phys. Chem. Solid* **1958**, *4*, 241. 304
54. Moriya, T. Anisotropic Superexchange Interaction and Weak Ferromagnetism. *Phys. Rev.* **1960**, *120*, 91. 305
55. Mühlbauer, S.; Binz, B.; Jonietz, F.; Pfleiderer, C.; Rosch, A.; Neubauer, A.; Georgii, R.; Böni, P. Skyrmion Lattice in a Chiral Magnet. *Science* **2009**, *323*, 915. 306
56. Huang, S.X.; Chien, C.L. Extended Skyrmion Phase in Epitaxial FeGe(111) Thin Films. *Phys. Rev. Lett.* **2012**, *108*, 267201. 307
57. Zhuo, F., Sun, Z.Z. Field-driven Domain Wall Motion in Ferromagnetic Nanowires with Bulk Dzyaloshinskii-Moriya Interaction. *Sci. Rep.* **2012**, *6*, 25122. 308
58. Fert, A.; Cros, V.; Sampaio, J. Skyrmions on the track. *Nat. Nanotechnol.* **2013**, *8*, 152. 309
59. Chen, G.; Zhu J.; Quesada, A.; Li, J.; N'Diaye, A.T.; Huo, Y.; Ma, T.P.; Chen, Y.; Kwon, H.Y.; Won, C.; Qiu, Z.Q.; Schmid, A.K.; Wu, Y.Z. Novel Chiral Magnetic Domain Wall Structure in Fe/Ni/Cu(001) Films. *Phys. Rev. Lett.* **2013**, *110*, 177204; Chen, G.; Ma, T.; N'Diaye, A.T.; Kwon, H.; Won, C.; Wu, Y.; Schmid, A.K. Tailoring the chirality of magnetic domain walls by interface engineering. *Nat. Commun.* **2013**, *4*, 2671. 310
60. Torrejon, J.; Kim, J.; Sinha, J.; Mitani, S.; Hayashi, M.; Yamanouchi, M.; Ohno, H. Interface control of the magnetic chirality in CoFeB/MgO heterostructures with heavy-metal underlayers. *Nat. Commun.* **2014**, *5*, 4655. 311
61. Tacchi, S.; Troncoso, R.E.; Ahlberg, M.; Gubbiotti, G.; Madami, M.; Akerman, J.; Landeros, P. Interfacial Dzyaloshinskii-Moriya Interaction in Pt/CoFeB Films: Effect of the Heavy-Metal Thickness. *Phys. Rev. Lett.* **2017**, *118*, 147201. 312
62. Belabbes, A.; Bihlmayer, G.; Bechstedt, F.; Blügel, S.; Manchon, A. Hund's Rule-Driven Dzyaloshinskii-Moriya Interaction at 3d-5d Interfaces. *Phys. Rev. Lett.* **2016**, *117*, 247202. 313

63. Nawaoka, K.; Miwa, S.; Shiota, Y.; Mizuochi, N.; Suzuki, Y. Voltage induction of interfacial Dzyaloshinskii–Moriya interaction in Au/Fe/MgO artificial multilayer. *Appl. Phys. Express* **2015**, *8*, 063004. 339
340
64. Gilbert, T.L. A phenomenological theory of damping in ferromagnetic materials. *IEEE Trans. Magn.* **2004**, *40*, 40, 3443. 341
65. Bogdanov, A.N.; Rößler, U.K. Chiral Symmetry Breaking in Magnetic Thin Films and Multilayers. *Phys. Rev. Lett.* **2001**, *87*, 037203. 342
66. Moon, J.H.; Seo, S.M.; Lee, K.J.; Kim, K.W.; Ryu, J.; Lee, H.W.; McMichael, R.D.; Stiles, M.D. Spin-wave propagation in the presence of interfacial Dzyaloshinskii-Moriya interaction. *Phys. Rev. B* **2013**, *88*, 184404. 343
344
67. Di, K.; Zhang, V.L.; Lim, H.S.; Ng, S.C.; Kuok, M.H.; Qiu, X.; Yang, H. Asymmetric spin-wave dispersion due to Dzyaloshinskii-Moriya interaction in an ultrathin Pt/CoFeB film. *Appl. Phys. Lett.* **2015**, *106*, 052403. 345
346
68. Manchon, A.; Ndiaye, P.; Moon, J.H.; Lee, H.W.; Lee, K.J. Magnon-mediated Dzyaloshinskii-Moriya torque in homogeneous ferromagnets. *Phys. Rev. B* **2014**, *90*, 224403. 347
348
69. Vansteenkiste, A.; Leliaert, J.; Dvornik, M.; Helsen, M.; Garcia-Sanchez, F.; Van Waeyenberge, B. The design and verification of MuMax3. *AIP Adv.* **2014**, *4*, 107133. 349
350
70. Klingler, S.; Chumak, A.V.; Mewes, T.; Khodadadi, B.; Mewes, C.; Dubs, C.; Surzhenko, O.; Hillebrands, B.; Conca, A. Measurements of the exchange stiffness of YIG films using broadband ferromagnetic resonance techniques. *J. Phys. D: Appl. Phys.* **2015**, *48*, 015001. 351
352
353
71. Klos J.W.; Gruszecki, P.; Serebryannikov, A.E.; Krawczyk, M. All-Angle Collimation for Spin Waves. *IEEE Magn. Lett.* **2015**, *6*, 3500804. 354
355
72. Gruszecki, P.; Romero-Vivas, J.; Dadoenkova, Y.S.; Dadoenkova, N.N.; Lyubchanskii, L.; Krawczyk, M. Goos-Hänchen effect and bending of spin wave beams in thin magnetic films. *Appl. Phys. Lett.* **2014**, *105*, 242406; Gruszecki, P.; Dadoenkova, Y.S.; Dadoenkova, N.N.; Lyubchanskii, I.L.; Vivas, J.R.; Guslienko, K.Y.; Krawczyk, M. Influence of magnetic surface anisotropy on spin wave reflection from the edge of ferromagnetic film. *Phys. Rev. B* **2015**, *92*, 054427; Gruszecki, P.; Mailyan, M.; Gorobets, O.; Krawczyk, M. Goos-Hänchen shift of a spin-wave beam transmitted through anisotropic interface between two ferromagnets, *Phys. Rev. B* **2017**, *95*, 014421. 356
357
358
359
360
361
73. Sanchez, F.G.; Borys, P.; Vansteenkiste, A.; Kim, J.V.; Stamps, R.L. Nonreciprocal spin-wave channeling along textures driven by the Dzyaloshinskii-Moriya interaction. *Phys. Rev. B* **2014**, *89*, 224408. 362
363
74. Lee, S.J.; Moon, J. H.; Lee, H.W.; Lee, K.J. Spin-wave propagation in the presence of inhomogeneous Dzyaloshinskii-Moriya interactions. *Phys. Rev. B* **2017**, *96*, 184433. 364
365
75. Korner H.S.; Stigloher, J.; Back, C.H. Excitation and tailoring of diffractive spin-wave beams in NiFe using nonuniform microwave antennas. *Phys. Rev. B* **2017**, *96*, 100401(R). 366
367
76. Wang, H.; Flacke, L.; Wei, W. *et. al.* Sub-50nm wavelength spin waves excited by low-damping Co₂₅Fe₇₅ nanowires. *Appl. Phys. Lett.* **2021**, *119*, 152402. 368
369
77. Janson, O.; Rousochatzakis, I.; Tsirlin, A. *et. al.* The quantum nature of skyrmions and half-skyrmions in Cu₂OSeO₃. *Nat. Commun.* **2014**, *5*, 5376. 370
371
78. Qian, F.; Bannenberg, L.; Wilhelm, H. *et.al.* New magnetic phase of the chiral skyrmion material Cu₂OSeO₃. *Sci. Adv.* **2018**, *4*, eaat7323. 372
373
79. Deng, L. Z.; Wu, H.C.; Litvinchuka, A.P. *et. al.* Room-temperature skyrmion phase in bulk Cu₂OSeO₃ under high pressures. *Proc. Natl. Acad. Sci.* **2020**, *117*, 8783. 374
375
80. Avci, C.O.; Rosenberg, E.; Caretta, L.; Büttner, F.; Mann, M.; Marcus, C.; Bono, D.; Ross, C.A.; Beach, G.S.D. Interface-driven chiral magnetism and current-driven domain walls in insulating magnetic garnets. *Nat. Nanotechnol.* **2019**, *14*, 561. 376
377
81. Caretta, L.; Rosenberg, E.; Büttner, F.; Fakhru, T.; Gargiani, P.; Valvidares, M.; Chen, Z.; Reddy, P.; Muller, D.A.; Ross, C.A.; Beach, G.S.D. Interfacial Dzyaloshinskii-Moriya interaction arising from rare-earth orbital magnetism in insulating magnetic oxides. *Nat. Commun.* **2020**, *11*, 1090. 378
379
380
82. Ding, S.; Baldrati, L.; Ross, A.; Ren, Z.; Wu, R.; Becker, S.; Yang, J.; Jakob, G.; Brataas, A.; Kläui, M. Identifying the origin of the nonmonotonic thickness dependence of spin-orbit torque and interfacial Dzyaloshinskii-Moriya interaction in a ferrimagnetic insulator heterostructure. *Phys. Rev. B* **2020**, *102*, 054425. 381
382
383